On the relation between GPS tropospheric gradients and the local topography

Laurent Morel, Ouafae Moudni, Frédéric Durand, Joëlle Nicolas, Stéphane Durand, Jean-Michel Follin, Eric Pottiaux, Joël van Baelen, Paulo Sergio de Oliveira

On the relation between GPS tropospheric gradients and the local topography

Laurent Morel[1], Ouafae Moudni[1], Frédéric Durand[1], Joëlle Nicolas[1], Jean Michel Follin[1], Stéphane Durand[1], Eric Pottiaux[2], Joël Van Baelen[3], Paulo Sergio de Oliveira Jr[4]

[1]GeF Laboratory, GRGS, ESGT - CNAM, Le Mans, France
[2]Royal Observatory of Belgium, Brussels, Belgium
[3]Laboratoire de l'Atmosphère et des Cyclones, CNRS/Université de La Réunion, Saint-Denis, France
[4]PPGCC/UFPR, Curitiba-PR, Brazil

Corresponding author: Laurent Morel (laurent.morel@lecnam.net)

Abstract. The estimation of tropospheric gradients in GNSS data processing is a well-known technique to improve positioning precision.

To study the correlation between the tropospheric gradients and the topography, we computed Zenith Wet Delay (ZWD) and tropospheric gradients using the GIPSY-OASIS II SOFTWARE from 2 years of GPS observations recorded at 52 worldwide permanent stations, focusing on regions with significant relief. We observe that gradient directions are stable over time and point towards the relief for most of the considered stations. Based on these results, we discuss the physical meaning of the tropospheric horizontal gradients and we investigate why gradients have this particular direction for stations located nearby high mountains. The GPS stations were selected and classified into four main categories: stations close to a mountain range or an isolated mountain (class 1 and 2), stations surrounded by isolated mountains in several directions or in all directions (class 3 and 4). The correlation between the gradient direction and their magnitude with respect to mountain slopes was analysed. A very clear correlation appears for stations of classes 1 and 2 whereas no correlation is obvious for stations of classes 3 and 4. For 89% of stations in classes 1 and 2, a relevant correlation appears, varying between 0.4 and 1. For 64% of stations in classes 1 and 2, a relevant correlation appears, varying between 0.6 and 1. Horizontal gradients estimation show very significant amplitude and a stable direction all along the year, this main direction is most of the time pointing towards the direction of mountains. This behaviour can be explained by a vertical shift of the tropospheric layer due to the presence of mountains, close to the station and up to the maximum distance of 60 km from the station. This orientation does not seem to depend on seasons because no annual or bimonthly means variations appear for all stations. Moreover diurnal variations do not appear on the spatial distribution of the gradients and results are similar for neighbouring stations, separated by few km, which show that local effects such as multipath propagation have influence.

Keywords : GNSS, Zenith tropospheric delay, Zenith wet delay, tropospheric gradients

1 Introduction

Taking into account the propagation delay of electromagnetic wave signals due to the troposphere is mandatory in space geodetic techniques such as Global Navigation Satellite Systems (GNSS). This tropospheric delay has to be mitigated by using a model such as those recommended in the IERS Conventions 2010 (Petit and Luzum, 2010). These models are usually expressed as a function of elevation (el) and azimuth (Az) of the satellite as in Eq. (1):

$$STD = ZHD.mf_H(el) + ZWD.mf_W(el) + mf_G.\left(G_N.\cos(Az) + G_E.\sin(Az)\right) \quad (1)$$

The total tropospheric delay observed at the zenith of a GNSS station, i.e. the Zenith Total Delay (ZTD), is divided into the Zenith Hydrostatic Delay (ZHD) and the Zenith Wet Delay (ZWD), which respectively represent about 90 % and 10 % of the total delay. The third part of tropospheric model accounts for the azimuthal anisotropy of tropospheric delay by introducing the two horizontal components of the gradient, i.e. its decomposition in the North-South (G_N) and the East-West (G_E) directions. The hydrostatic and wet delays and the horizontal gradients are mapped down to any elevation angle *el* using the corresponding hydrostatic, wet and gradient mapping functions (mf_H , mf_W and mf_G respectively) to provide the Slant Total Delay (STD), i.e. the delay in the satellite direction. In these tropospheric models, the ZHD and the mapping functions are assumed to be known a priori (i.e. modelled) while the ZWD and the horizontal gradient components are estimated. Several studies have shown that the estimation of tropospheric horizontal gradients benefits positioning using spatial geodetic techniques (Bar-Sever et al., 1998; Chen and Herring, 1997; Iwabuchi et al, 2003; MacMillan, 1998; Tregoning et al, 1998; Willis et al., 2012, Zhou et al., 2017).

In the recent past years, several authors have focused their studies on tropospheric gradients. By studying 102 worldwide permanent stations well distributed in latitude, Meindl et al. (2004) established that the mean annual value of the north gradient component G_N is positive for all the stations in the southern hemisphere and negative for those in the northern hemisphere, corresponding to gradient vectors pointing towards the Earth's equator. They highlighted that this general gradient behaviour reflects the trend of increasing atmospheric water vapour content when moving towards the Earth's equator. They suggested that "it is "remarkable that such a global troposphere variation can be well detected by a GPS station with its restricted tropospheric field of view with a radius of about 200 km".

Dousa et al (2016) noted that "GNSS-derived gradients demonstrated a nice ability for producing a homogeneous tropospheric gradient field revealing details in the actual state of the troposphere". Gradients were estimated with two GNSS software packages and two NWM global models and showed discrepancies in terms of the magnitude of gradient values while keeping consistency in directions. More interesting details could be observed in GNSS maps instead they are note visible or smoothed in NWM maps.

Recently, Zus et al. (2019a) demonstrated that ZWD interpolation can be improved by utilizing tropospheric gradients. Moreover, Zus et al (2019b) showed that the assimilation of the tropospheric gradients in addition to the ZTDs improves the

refractivity field in the vicinity of the considered station. Both studies provide clear evidence that tropospheric gradients contain information on the water vapor distribution in the troposphere.

Kacmarik et al. (2019) analysed the behaviour of the tropospheric gradients estimation. They showed, firstly, that adding low-elevation GNSS data increase the robustness of the gradient estimation, secondly a weak impact of adding Glonass data on top of GPS observations, and finally a high sensitivity of real time gradients estimation to mapping functions. Furthermore, Heki et al. (2019) demonstrated that, at Japanese coastal stations, the sea breeze induces landward gradients in summer daytime and stationary southward gradients in winter due to their dominating dry component with a latitude dependence of surface pressure.

The current study is a follow-up to an earlier local study performed in Corsica (Morel et al., 2014). In this previous paper, we studied the temporal and spatial distribution of horizontal tropospheric gradients estimated over one year (2011) at 13 permanent stations in Corsica Island (France). We demonstrated the correlation of the horizontal gradient amplitude with the temporal distribution of the water vapour all along the year 2011. Their amplitudes were very significant and their directions were stable all along the year for most of the stations. Their direction is most of the time pointing towards inland, in the opposite direction of the largest downslope and perpendicular to the coastline. These first results gave an indication of the physical behaviour of the horizontal gradients but the origin of such directions required further investigations.

In this paper, we study the temporal and spatial distribution of horizontal tropospheric gradients estimated over one year (2015 and 2016) at 52 permanent stations distributed all around the world. Our main motivation is to analyse the gradients estimated during the GNSS data processing in order to investigate their physical interpretation (Bock et al, 2008; Brenot et al., 2013; Dousa et al., 2017). Our second goal is to investigate the possible systematic behaviour of the tropospheric gradients in mountainous areas. We study their correlation with the geographical context, particularly the environmental contrast between the continent and the sea and the very large topography variations that cause humidity content spatial variations, local sea breeze and land wind regimes (Heki et al, 2019). Considering that humidity is concentrated in the troposphere near the surface (up to 3 km) and taking into account signals coming from satellites with a cut-off angle of 3 degrees, the horizontal gradient behaviour can be influenced by the humidity pattern distribution within a distance from the station up to 57 km.

The paper is organized as follows: we first describe our methodology to study a potential correlation between the gradient direction and the presence of mountains in the tropospheric field of view of the considered GPS station, up to 60 km. Then, the GPS data and data processing methods used to estimate the tropospheric parameters (ZWD and horizontal gradients) based on PPP (Precise Point Positioning) technique with the GIPSY-OASIS software (Zumberge et al., 1997) are presented. Finally, the tropospheric gradients correlation with the relief is analysed and discussed.

2 Data and methods

2.1 GPS data

To analyse the correlation between the gradient direction and the relief around the GPS stations, we applied our methodology to 52 permanent stations distributed around the world. Several criteria have been considered to select them: sites with strong contrast between plain and mountain, close enough to the mountains (up to 60 km), and different mountain location directions relative to the station. In order to analyse the relief effect on the gradients direction, only sites with significant topographic height contrasts close to the GPS stations have been considered, with a minimum height difference of over 500 m between the station elevation and the highest point of the surrounding mountains.
Then, the stations have been classified into four categories: class 1 for stations close to a mountain range, class 2 for stations close to an isolated mountain, class 3 for stations surrounded by isolated mountains in several directions and class 4 for stations surrounded by mountains in all the directions. Table 1 summarises the number of stations in each class and Fig. 1 presents the spatial distribution of these permanent stations.

Table 1. Number of GPS stations considered in each class.

Classes	Class 1	Class 2	Class 3	Class 4
Number of stations	24	12	10	6

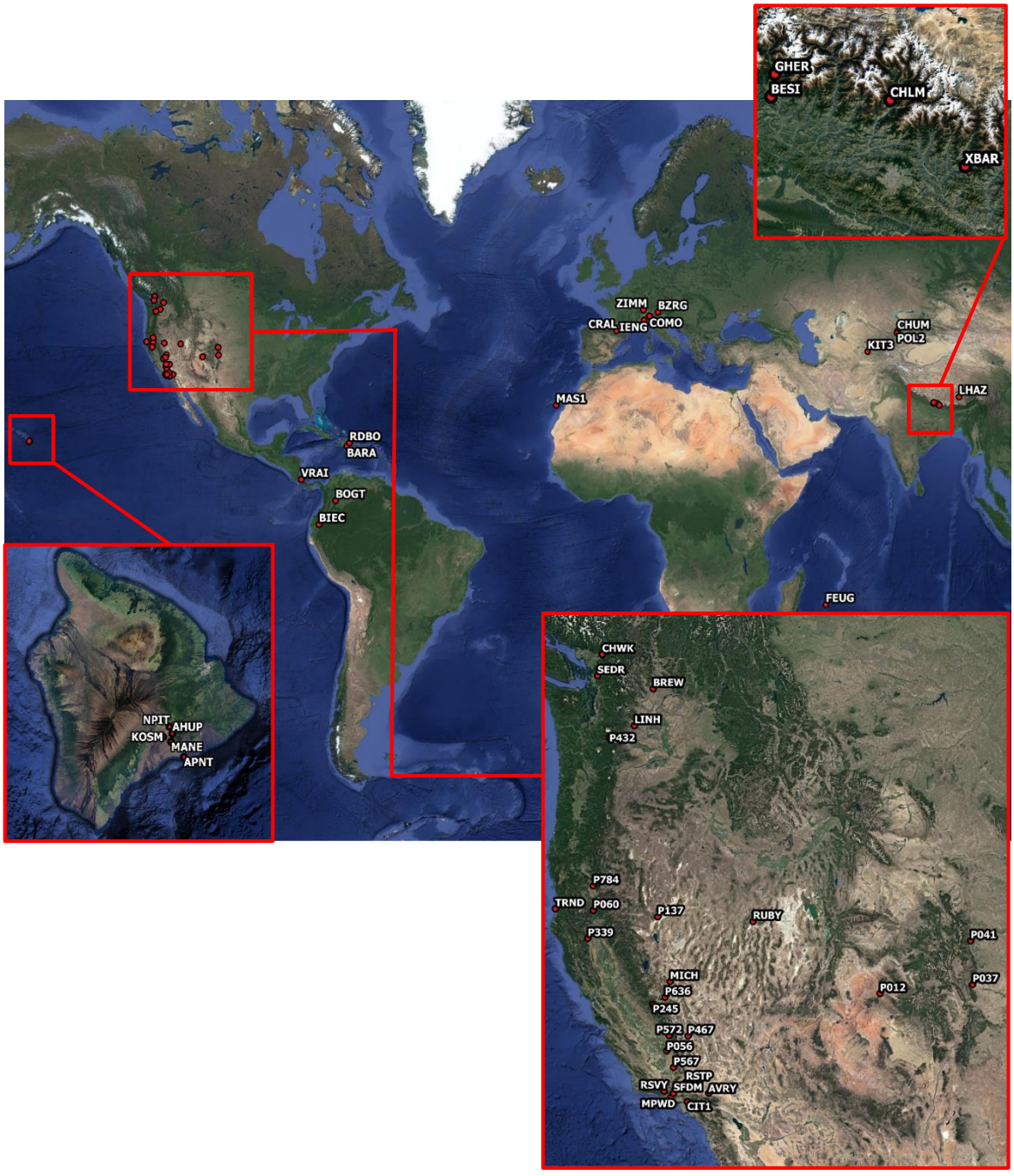

Fig. 1. Map of the 52 permanent GPS stations considered with a zoom on three particular areas. © Google Maps.

2.2 Methodology

In a first step, the horizontal gradients are estimated each 5 min, and then averaged over 1 hour all along the year 2015. They are plotted as a point cloud corresponding to their annual spatial distribution, for the CRAL station shown in Fig. 2 as an example. Each point corresponds to the gradient north component as a function of the gradient east component. Then, the sum of the points in each 30° sector is computed and is affected to the corresponding sector. On an azimuthal plot centred on the considered GNSS station, the points affected to the different sectors are drawn at a distance from the centre proportional to the sum affected to the sector. Then, the points are connected by a red curve as shown on Fig. 3, to represent the spatial distribution of the gradients as a radar plot. A similar curve would have been obtained if we had considered the gradient intensity instead of the gradient counting because all the clouds are isotropic as in Fig. 2. We privileged counting for the purpose of simplicity and because it would have been more or less arbitrary to class the intensity of the points.

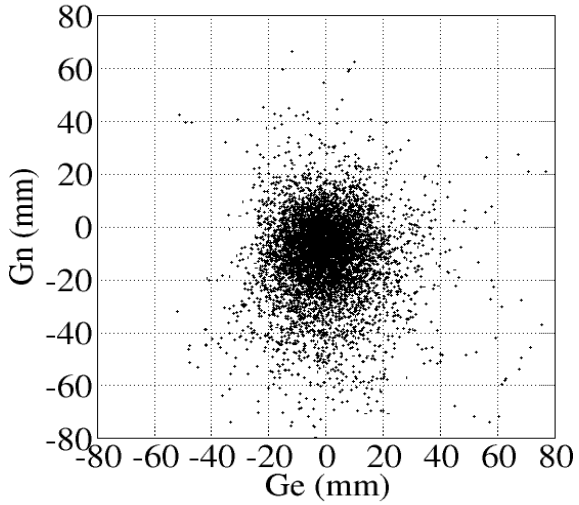

Fig. 2. Spatial distribution of the horizontal gradients along the year 2015 for the station CRAL located in French Pyrenees. The origin corresponds to the location of the GNSS permanent station.

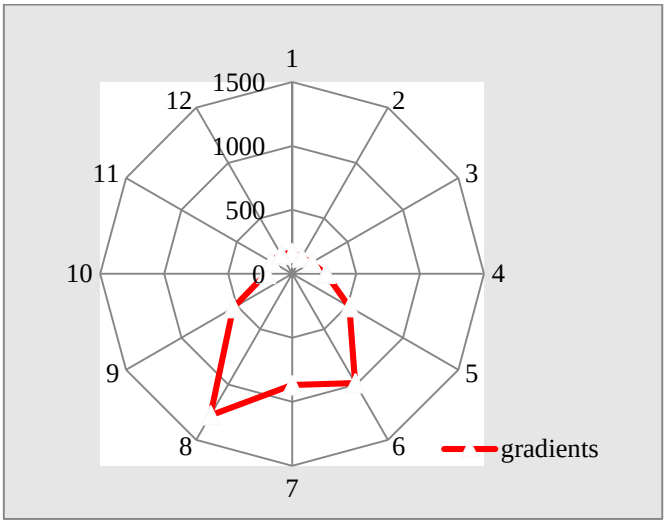

Fig. 3. Spatial distribution of the horizontal gradients along the year 2015 for the station CRAL located in French Pyrenees. The cloud points are counted in each 30° azimutal sector and represented by their sum. All the points are connected by a red curve to represent the spatial distribution.

In a second step, to represent the relief around the GNSS station, the highest terrain elevation is determined for each azimuth sector, 30° by 30°. For that we use the Earth digital elevation model GTOPO15 from the SRTM v2 mission (Farr et al, 2007), with a resolution of 500 m after conversion. To identify the highest elevation point in all directions, three curves are drawn corresponding to three different distances from the station, 20, 40 and 60 km respectively, as illustrated in Fig. 4. In each sector of this figure, the distance from the centre is proportional to the height difference between the GNSS station and the height of the highest elevation point. Four circles are drawn to represent 1000 m, 2000 m, 3000 m and 4000 m height differences. Moreover, tests showed that a finer azimuth step doesn't lead to significant differences in the results.

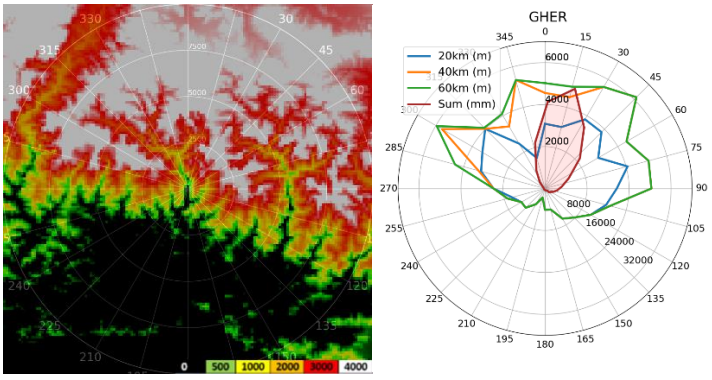

Fig. 4. Example of relief around the GHER station located in Himalaya (class 1). The spatial distribution of the relief is represented by three curves (blue, orange and green) corresponding to three distances from the station (20, 40 and 60 km) to identify the highest elevation point in all the directions. Distance from the centre is proportional to the height difference between the station elevation and the highest elevation point. The four circles drawn represent height differences of 2000 m, 4000 m and 6000 m respectively.

Finally, gradient and relief curves are superimposed on the same plot (Fig. 5) to perform a visual analysis of the correlation between the orientation of the horizontal gradients and the relief. When the gradient and relief curves have a similar pattern, it means that the gradients have a privileged direction and a strong correlation with the relief around the station. We then computed the correlation coefficients between the gradient direction values and the highest elevation in each sector by using the sample Pearson correlation coefficient. Three correlation coefficients are obtained for the relief at three considered distances: 20 km, 40 km, 60 km.

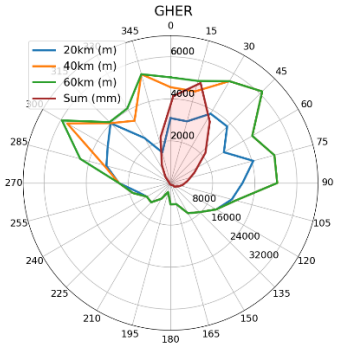

Fig. 5. Gradient orientation curve (red) and relief curves (blue, orange and green) around the station GHER located in Himalaya considering three distances from the station (20, 40 and 60 km) for the relief representation.

2.3 GPS data processing

The data processing was done with the PPP technique using the GIPSY/OASIS 6.4 software (Bertiger et al, 2010) for all the stations all along the years 2015 and 2016. The observation cut-off angle was set to 3 degrees in order to study the spatial distribution of the water vapour with the horizontal gradients (Willis et al., 2012). We used the JPL final products (Earth orientation parameters, orbits and clocks), no atmospheric pressure loading correction and the igs08 antenna calibration model (Dow et al, 2009, Schmid et al., 2007). We followed the recommendations from the IERS Conventions 2010 (Petit and Luzum, 2010) for the tropospheric modelling: we used the a priori Vienna ZHD (VZHD) and the Vienna Mapping Function (VMF1) derived from Numerical Weather Model (NWM) data and provided by the Vienna University of Technology (Boehm et al., 2006). The processing strategy options are summarised in Table 2 and very similar to the one used in our first study in Corsica (Morel et al, 2014). The classic parameters for PPP were estimated: station position, receiver clocks, ZWDs, and horizontal tropospheric gradients. The ambiguity resolution is obtained behalf the additional products necessary for that (wide-lane phase bias files from JPL) (Bertiger et al., 2010). The tropospheric parameter is estimated using a random walk process at an interval of 5 min, i-e. the same as the measurement data rate since this software is using a Kalman filter solution. Results have been averaged over 1-hour-time bins. The 1-hour interval averaging was chosen because it is suitable to study the behaviour of gradients throughout days, months and years. Point by point variations allowed for ZWD (1 cm/$\sqrt{hour}$) and for gradients at zenith (0.03 cm/$\sqrt{hour}$), which corresponds for gradients to 1 cm/$\sqrt{hour}$ at 10°, have been chosen. In our first article (Morel et al., 2014), data was also processed with the double difference technique using the GAMIT software and the yearly average of the horizontal gradients estimated by the two software were in good agreement. In this article, we keep only the GIPSY software because it was necessary to be able to process stations all around the world and sometimes isolated. A double difference process would have needed several sub network processing which would have limited the number of stations to be studied whereas it was difficult to find a lot of them.

Table 2. Summary of the processing options used to compute the tropospheric parameters with the GIPSY-OASIS 6.4 software.

Observations		GPS only
Parameter estimation		Precise Point Positioning stochastic estimation (clocks, troposphere)
Station Coordinates		Fixed
Ambiguity resolution		Yes
Earth Orientation Parameters		IERS standards 2010
Orbit and Clocks products		JPL
Atmospheric loading correction		no
Elevation cut-off angle		3°
Antenna calibration (satellite and station)		IGS08.atx
ZHD	Delay model	VZHD
	Mapping functions	VMF
ZWD estimation	Interval	5 min
	Constraint	no
	Variation	1 cm / sqrt(h)
	Mapping function	VMF
Gradient estimation	Interval	5 min
	Constraint	no
	Variation	0,03 cm / sqrt(h)
	Mapping function	Bar Sever, 1998
		VMF.cot(el)

3 Results

3.1 Representative results

In this part, we illustrate the results with representative cases for each class defined in section 2.1. Fig. 6 shows representative results for ‘class 1’ stations: GHER, POL2, P572 and P467. These stations have significant mountains in different directions: towards the north for GHER, the south for POL2, the east for P572 and the west for P467. A visual correlation can be observed for all these stations whatever the direction of the mountains. Gradient curves in blue (filled with pink) have a very well identified orientation towards the highest elevation point, regardless of its distance from the station considered for the identification of the highest elevation point. The correlation coefficients between the gradient direction

and the relief at 20 km, 40 km and 60 km are 0.50, 0.63 and 0.67 respectively for GHER station (0.74, 0.73 and 0.68 for POL2; 0.81, 0.85 and 0.77 for P572; 0.58, 0.65 and 0.71 for P467). POL2 and P572 show stronger correlation because mountains are very well identified in a specific direction: south for POL2 and east for P572. The front of mountains appears larger and less oriented for GHER, and some little mountains exist also in the opposite direction of the main mountain for P467, which can explain lesser correlation for both stations. A marked increase of the correlation coefficients with respect to the distance of relief from the station is clear for GHER and P467 stations, while the correlation coefficients appear more or less constant for POL2 and P572. Again, it can be explained by the previous reasons even if the differences are not very significant. Since similar results have been retrieved for stations in class 2 whatever the isolated mountains direction, we do not show them here.

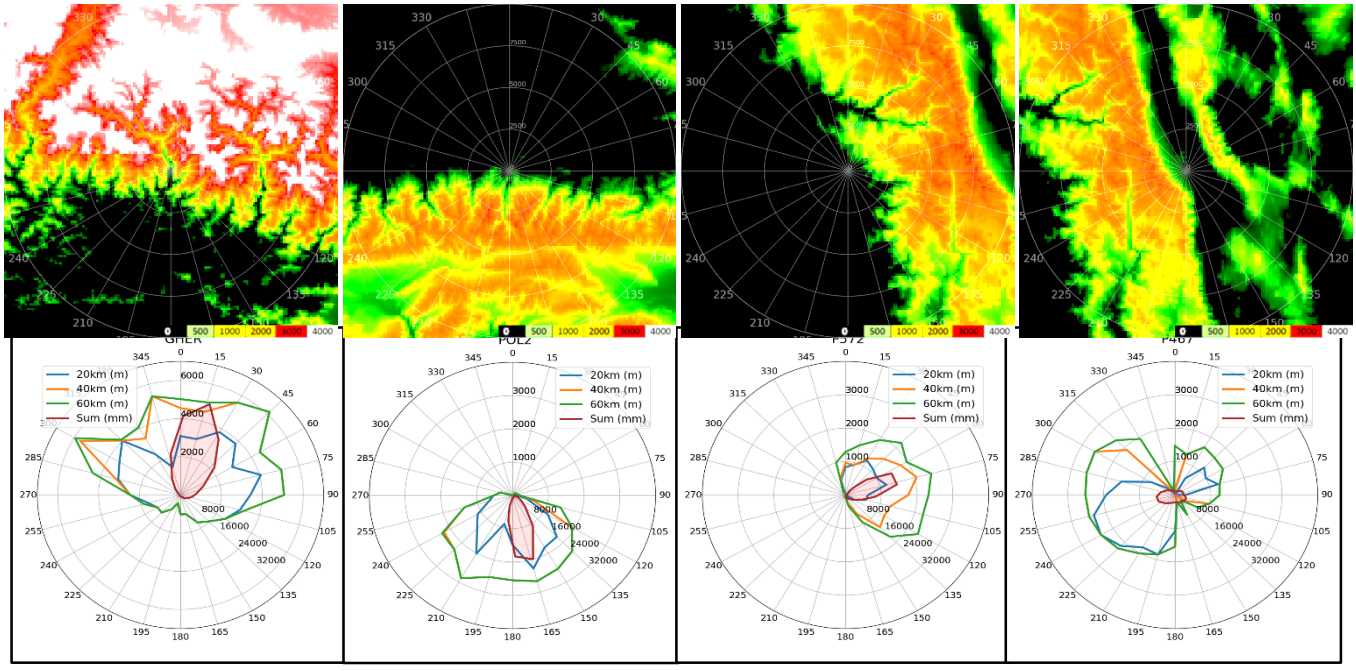

Fig. 6. Relative location of mountains from the station (top charts). Gradients and relief curves (bottom radar charts centred on station location) for class 1 stations: GHER (Himalaya), POL2 (Nepal), P572 and P467 (California near Sierra Nevada). Red curve (filled with pink) represents the gradient and the other curves represent the relief at different distances from the station: blue for 20 km, orange for 40 km and green for 60 km. Y axis legend corresponds to the elevation in m. (scale is different for GHER as it is situated in Himalaya, with height difference up to 6 km). Other axis legend (at 135° azimuth) corresponds to the sum of gradient.

In Fig. 7, no preferred direction can be noticed for the station MICH located in California near Sierra Nevada and belonging to class 3, which corresponds to a station relatively surrounded by isolated mountains. Gradient points are scattered in all

directions and the gradient curve is not well identified. The correlation coefficients between the gradient direction and the relief at 20 km, 40 km and 60 km are 0.71, 0.21 and 0.04 respectively. We can do similar comment for the station BZRG located in Italia near Dolomites and belonging to class 4 which correspond to stations surrounded by mountains in all the directions (Fig. 8). Even if the gradient curve is a little better identified than for MICH station, it shows a symmetrical shape around the station. For this station, the correlation n coefficients between the gradient direction and the relief at 20 km, 40 km and 60 km are 0.10, 0.17 and 0.63 respectively. This station illustrates the typical results obtained for stations in class 4. In these two previous classes 3 and 4, it is not surprising that no correlation appears since the surrounding mountains have no preferred direction with respect to the station.

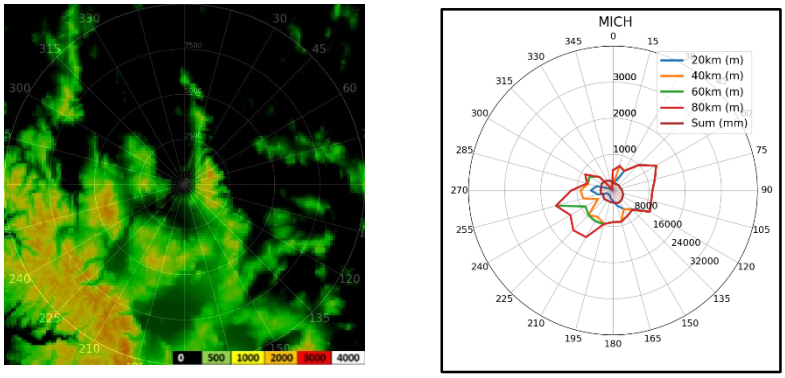

Fig. 7. Location of mountains relative to the ‘class 3’ GNSS station MICH located in California near the Sierra Nevada (left). Horizontal gradient and relief curves (right). Red curve (filled with pink) represents the gradient and the other curves represent the relief at different distances from the station: blue for 20 km, orange for 40 km and green for 60 km. Y axis legend corresponds to the elevation in m. Other axis legend (at 135° azimuth) corresponds to the sum of gradient.

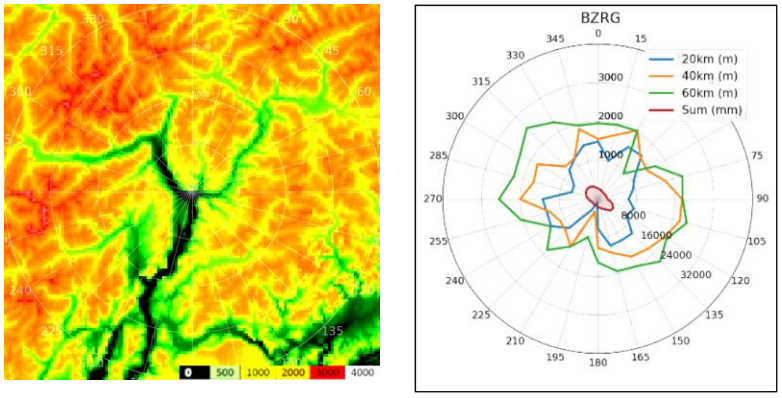

Fig. 8. Location of mountains relative to the 'class 4' GNSS station BZRG located in Italia near the Dolomites (left). Horizontal gradient and relief curves (right). Red curve (filled with pink) represents the gradient and the other curves represent the relief at different distances from the station: blue for 20 km, orange for 40 km and green for 60 km. Y axis legend corresponds to the elevation in m. Other axis legend (at 135° azimuth) corresponds to the sum of gradient.

3.2 Complete and statistical results

We computed the radar charts with the horizontal gradient and the relief curves and the corresponding correlation coefficients, for all the 52 considered permanent stations, between gradient direction and the relief at 20 km, 40 km and 60 km. For all stations and for each class, Table 3 presents the number of stations and the mean correlation coefficient between the gradient's direction and the relief for the different distances from the considered stations to identify the highest elevation point (20, 40 and 60 km). A very clear correlation appears for stations of class 1 and 2 whereas no correlation is obvious for stations of classes 3 and 4.

Table 3. Mean correlation coefficients between the tropospheric gradient orientation and the highest elevation point direction for each class of relief. The number of stations considered for each class is also indicated.

		number	Mean correlation coefficient		
			20 km	40 km	60 km
All stations		52	0.36	0.41	0.41
Type of relief	class 1	24	0.44	0.60	0.64
	class 2	12	0.62	0.64	0.68
	class 3	10	0.00	-0.03	-0.14
	class 4	6	0.17	-0.05	-0.06

Figure 9 shows the correlation coefficients for all the stations of class 1 and 2 (36 stations) only considering the distance of 60 km from the stations to identify the highest elevation point. Very similar curves are observed for the other distances from the stations. For 89% of stations of class 1 and 2, a correlation between 0.4 and 1 was found, and 64% of stations presented a correlation between 0.6 and 1. For these 36 stations, the correlation coefficients range between 0.4 and 1 except for 4 stations (P041, P636, SEDR, CIT1) and range between 0.6 and 1 except for 5 additional stations (LINH, P037, P339, MAS1, RSVY).

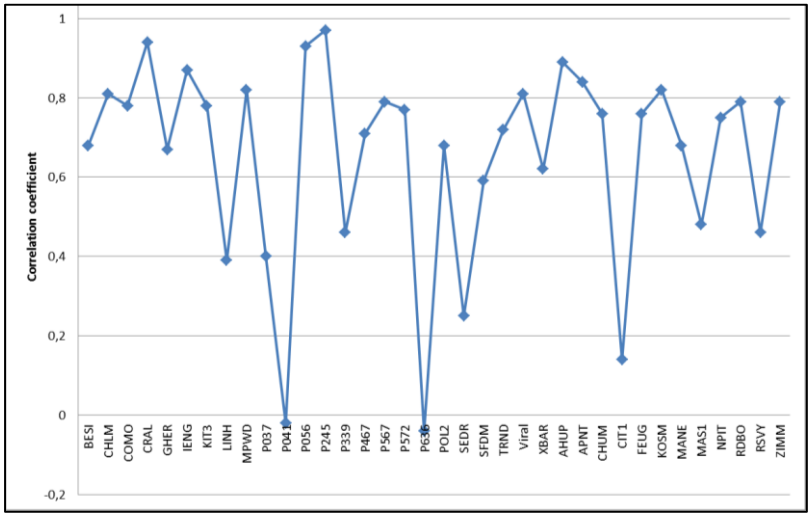

Fig. 9. Correlation coefficient for stations of class 1 and 2 between the gradient direction and the relief curves at 60 km from the station.

These complete results show clear correlation between gradient and relief due to the presence of mountains whatever the direction of the mountains.

4 Discussion

Our results clearly underline the influence of nearby mountains on the tropospheric gradient direction estimated from GPS data. In a preliminary study, realised before our previous article (Morel et al, 2014), gradients had been analysed for 10 stations in the Paris region (height variation < 200 m and far to the sea or mountains (> 200 km)). This preliminary study had shown no significant value for estimated gradient to allow us a statistical analysis. This influence of nearby mountains can probably be explained by a vertical shift of the tropospheric layer due to the presence of mountains, close to the station and up to the maximum distance of 60 km from the station as illustrated in Fig. 10. Then, the path delay through the troposphere is increased in the mountains direction and the lengthening depends on the mountains shape and altitude. If we consider the extreme case of a mountain range with a height difference of 3 km compared to the station elevation and a troposphere thickness of 3 km, this lengthening can reach twice as much compared to a station located in an area without relief (e.g. 114 km instead of 57 km for an elevation angle of 3 degrees). For an intermediate case (height difference of 2 km), as an isolated mountain, the extension is less important (e.g. 95 km instead of 57 km for an elevation angle of 3°) and stays significant even in the case shown in the Fig. 10 (76 km instead of 57 km for height difference of 1 km). Consequently, due to this path delay heterogeneity across the troposphere around the station, the tropospheric gradient should appear in the direction of the greatest path delay and thus of the highest relief. This particular gradient signature close to mountains can clearly be

observed in Kacmarick et al (2019). For Andes mountains, Tibetan Plateau and Rocky mountains, the figure A1 in the appendix A of this paper shows this behaviour of tropospheric gradient. High mountains in the vicinity of the respective stations change the 'tilting' of the troposphere, such that the mean tropospheric gradients do not point towards the equator but instead the mean tropospheric gradients point towards the mountain crests.

In the following parts, three tests have been performed to investigate this hypothesis.

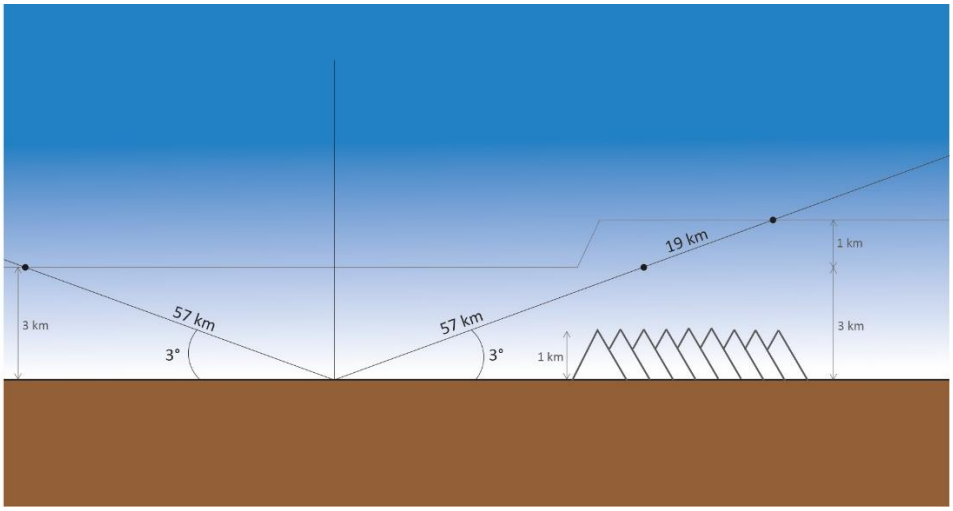

Fig. 10. Schematic path delay across troposphere of a GPS signal in the presence or not of mountains.

Firstly, an annual comparison of the results has been performed for 4 stations representative of class 1 (AHUP located in Hawai, COMO and IENG located in Italia near Alps and KIT3 located in Ouzbekistan near Hissar mount) and for 1 station of class 2 (KOSM located in Hawai), for the years 2015 and 2016. Table 4 presents the comparison of the correlation coefficients obtained for these 5 stations during each considered year.

Table 4. Correlation coefficients between the gradient direction and the relief for 5 stations for the years 2015 and 2016.

Stations		**Correlation in 2015**				**Correlation in 2016**			
	class	20 km	40 km	60 km	80 km	20 km	40 km	60 km	80 km
AHUP	**1**	0.94	0.88	0.89	0.74	0.89	0.92	0.89	0.68

COMO	**1**	0.91	0.81	0.79	0.77	0.89	0.75	0.78	0.73
IENG	**1**	-0.1	0.79	0.83	0.79	-0.05	0.86	0.87	0.81
KIT3	**1**	-0.15	0.14	0.78	0.9	-0.08	0.25	0.78	0.97
KOSM	**2**	0.98	0.87	0.82	0.66	0.98	0.89	0.82	0.64

Annual differences between these correlation coefficients are very weak and do not exceed 0.11, with a RMS of 0.05 for all the differences. This means that the correlation coefficients are very similar over these 2 years. Moreover, for all the considered stations, the radar charts match perfectly and no visual shift can be detected between the figures for the years 2015 and 2016. Since the gradient orientation is not dependent of the year, we can say that it corresponds to a systematic effect related to the environment around the station. Likewise, meteorological activities which are not similar every year seem to have no impact on the annual mean of gradient direction. Presence of mountains is the dominant effect. Considering that the differences of the correlation coefficients between these two years are not significant at all, no more stations were added to this specific study.

In order to go further in the tropospheric gradient behaviour analysis, we analysed monthly variations of their values for these 5 stations for the year 2016. Fig. 11 shows bimonthly means of the gradient sum counted in all the directions (30° by 30°). The relief around the stations is added (dashed line) considering the highest elevation point estimated at 60 km from the considered station.

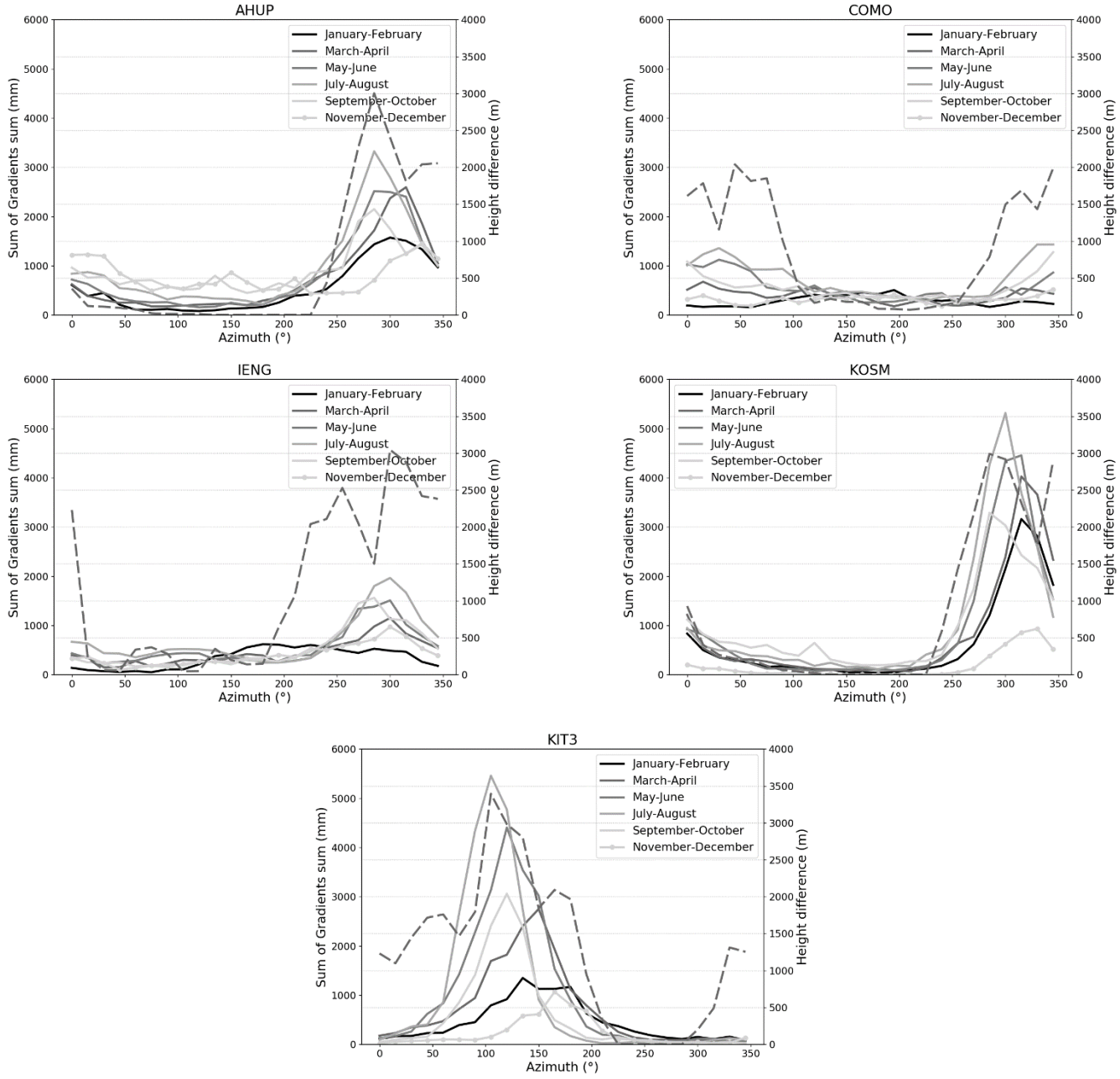

Fig. 11. Bimonthly variations of the mean tropospheric gradients sum all along the year 2016 for 5 stations. The dashed line represents the relief around the station estimated at 60 km from the station.

For all stations, no bimonthly means variations appear because all the bimonthly curves are correlated, less for KIT3. For this station, the sum of the gradients differs slightly according to the season, similar profiles are observed for all seasons. Likewise, for these 5 stations, the May-June and July-August profiles systematically show higher values due to the higher amount of water vapour during summer. Nevertheless, the systematic orientation of the gradients is always correlated with the relief for these 5 stations regardless to the seasons, which confirms the predominant effect of the mountains.

Considering that the gradient orientation could be related to the diurnal variation of humidity (Heki et al., 2019), daily variations were studied for all stations. For each considered station in Fig.12, we computed the averages of the gradient counting in each 30° sector separately during day (grey curve) and night (black curve) for all the year 2016. For easier interpretation, we added the topography (dashed line) around the stations considering the maximum altitude at 60 km from the station.

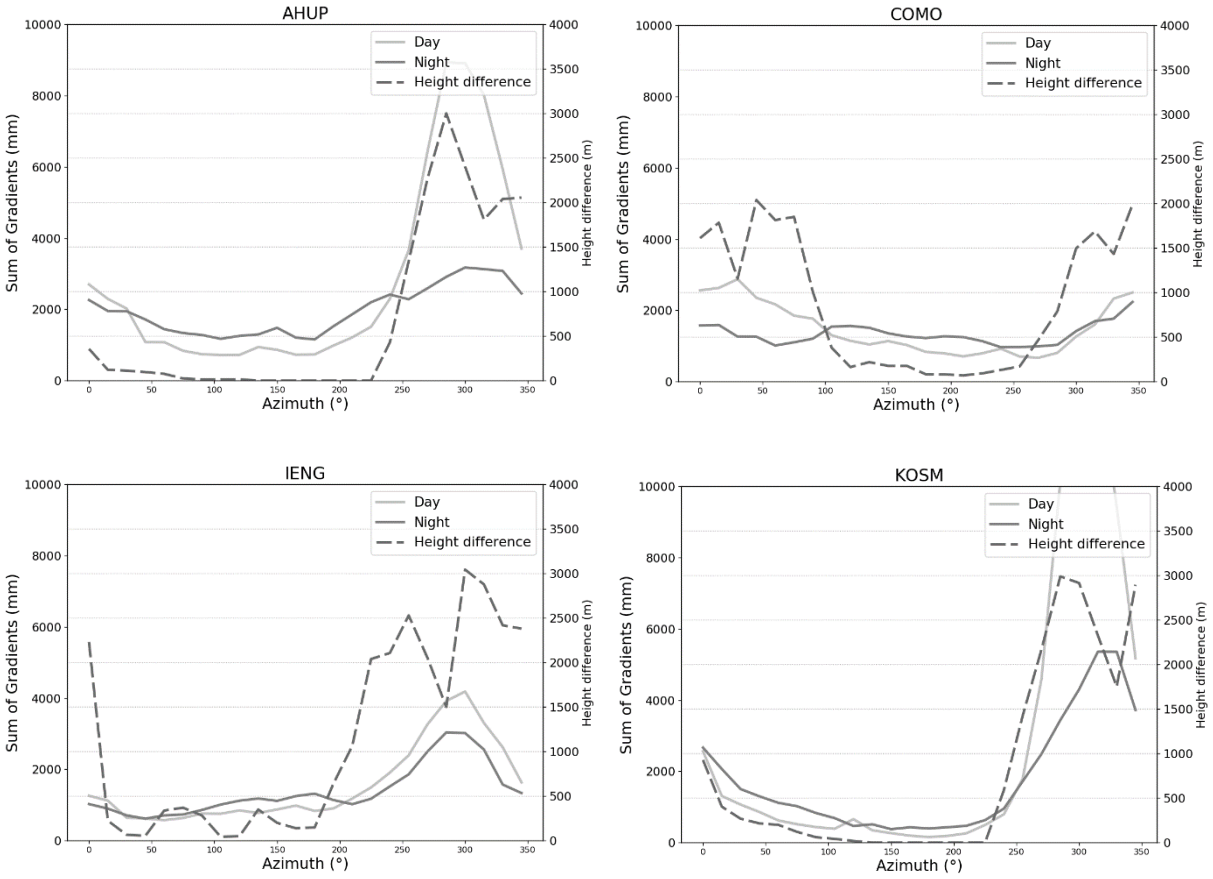

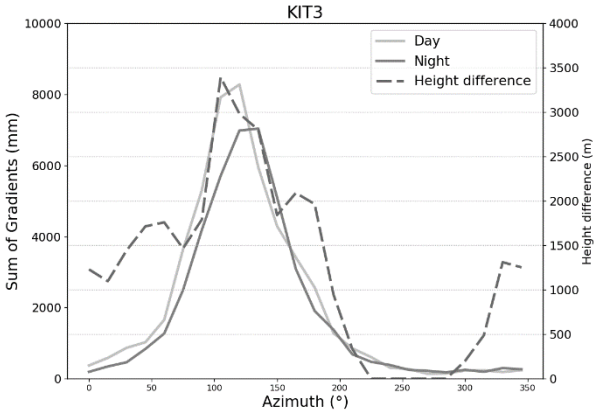

Fig. 12. Average of diurnal variations of gradients for 2016 for 5 stations. The dashed line represents the topography around the station at a distance of 60 km from the considered station.

For these 5 considered stations, the diurnal variations do not appear on the spatial distribution of the gradients because all the curves are correlated. Similar profiles are observed for all the stations and no gradient inversion is detected as in the study of Heki et al. (2019) where gradients are clearly dominated by local weather effects. For AHUP and KOSM, situated on the Hawai island, the sum of the day and night gradients are different but always with a higher amplitude in the direction of the relief. Even if no diurnal variations (AHUP) or weak diurnal variations (KOSM) are observed, these increase of gradient during the day could be explained by the water vapour locking by relief. The developments of clouds would be encouraged by the tropical convection and the trade winds.

In summary, the gradient shows a clear and systematic orientation towards the highest elevation point. This occurs due to the presence of mountains around the station. This orientation does not seem to depend on seasonal or daily weather effects. Meanwhile, other local effects such as multipath propagation could be responsible for this specific orientation. To analyse this potential effect, we analysed the tropospheric gradient behaviour of neighbouring stations (class 1 and 2). Fig. 13 shows radar charts for 3 pairs of stations (GHER and BESI located in Nepal near Himalaya, POL2 and CHUM located in Kazakhistan near the Alaa-Too mountains, KOSM and APNT located in Hawai,).

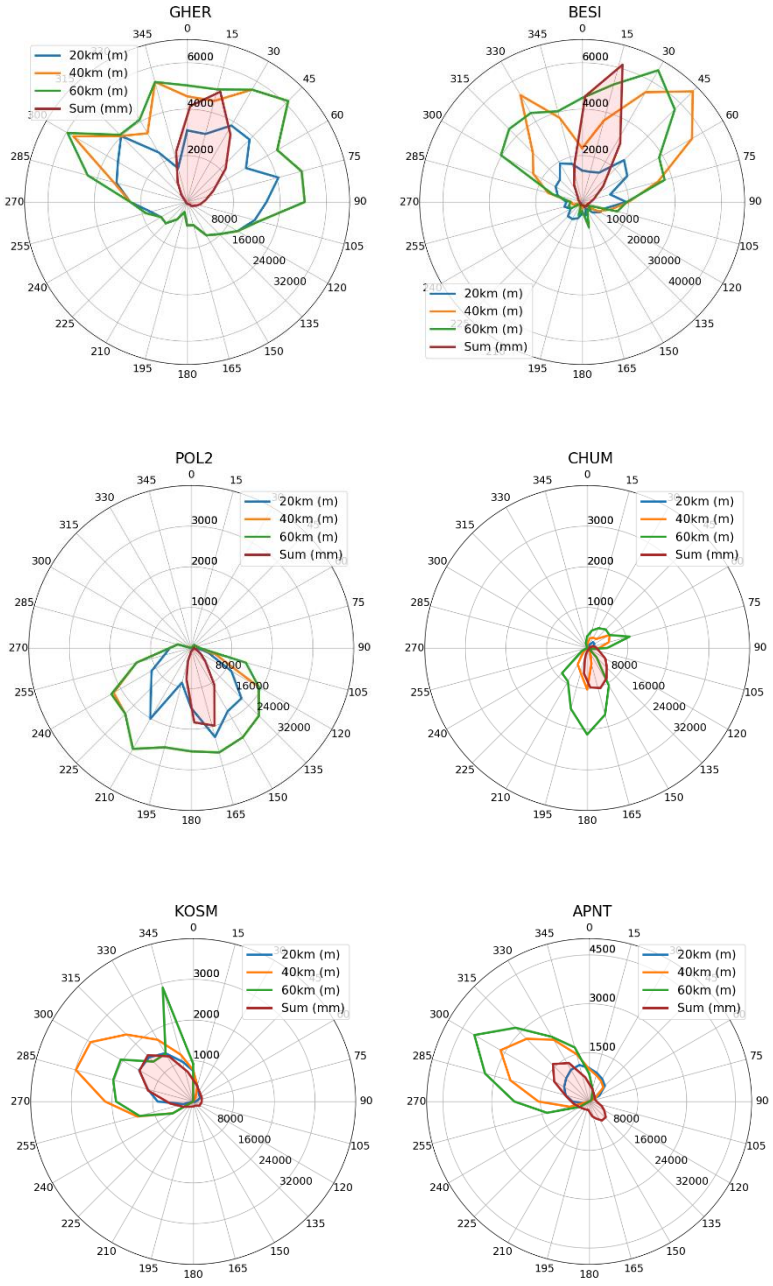

Fig. 13. Radar charts of gradient curve (red curve filled with pink) and relief curves (dark blue, orange and green curves) for 3 couple of neighbouring stations (GHER and BESI (class 1) located in Nepal near Himalaya; POL2 (class 1) and CHUM (class 2) located in Kazakhistan near Alaa-Too mountains; KOSM and APNT (class 2) located in Hawai).

BESI/GHER are separated by 18.7 km, POL2/CHUM by 35.7 km and KOSM/APNT by 16.3 km respectively. The gradient orientation is very similar for all these 3 pairs of stations, which means that if there is an effect of the multipath, it is not dominating. Even if this last test cannot be applied for all our 52 considered stations, these results confirm the influence of the mountains on the gradient orientation for these 6 particular stations and it does not deny these specific effects for the other stations.

5 Conclusions

By processing two complete years of GPS data (2015 and 2016) for 52 worldwide permanent stations, we studied the temporal behaviour and the spatial distribution of the horizontal tropospheric gradients. These gradients have been estimated using the GIPSY-OASIS software and the PPP processing method. The GPS stations were selected and classified into four main categories: stations close to a mountain range (class 1), stations close to an isolated mountain (class 2), stations surrounded by isolated mountains in several directions (class 3) and stations surrounded by mountains in all directions (class 4). The correlation between the gradients' direction and magnitude with respect to mountain slopes was analysed. A very clear correlation appears for stations of classes 1 and 2 whereas no correlation is obvious for stations of classes 3 and 4. For 89% of stations in classes 1 and 2, a relevant correlation appears, varying between 0.4 and 1. In fact, 64% of the stations in classes 1 and 2 presented strong correlation between 0.6 and 1. Horizontal gradients estimation show very significant amplitude and a stable direction all along the year, for most of the stations considered. This main direction is most of the time pointing towards the direction of mountains. This orientation does not seem to depend on seasonal or daily weather cycle. Additionally, we investigated local effects such as multipath propagation for some specific stations, and no local influence was found.

Results achieved in our study can at least reinforce that tropospheric horizontal gradients do have a particular behaviour according to the relief around the station location. A specific study is necessary to compute accurately how the mountains change the tilting of the troposphere, with theoric and simulation approaches in a first part, and with an experimental campaign in a second part. Furthermore their addition as parameters during GNSS data processing can be explored to improve GNSS positioning mathematical model. Thus, in further researches, the improvement on positioning with and without the gradients estimation for stations surrounded by mountains must be assessed. ZTDs are operationally assimilated into numerical weather prediction models and if this is not the case for the moment for the horizontal gradients, they are used now for the reconstruction of STD and these results are very promising for GNSS meteorology and climatology.

Acknowledgments

The authors acknowledge M. Florian Zus for scientific discussion. We are also grateful to all data and products providers without which this study wouldn't have been possible (JPL, IGS, UNAVCO).

References

Bar-Sever, Y.E., Kroger, P.M., and Borjesson, J.A.: Estimating horizontal gradients of tropospheric path delay with a single GPS receiver. J. Geophys. Res. 103(B3), 5019–5035, 1998.

Bertiger, W., Desai, S.D., Haines, B., Harvey, N., and Moore, A.W.: Single receiver phase ambiguity resolution with GPS data. J. Geod. 84(5), 327–337, 2010.

Bock, O., Bouin, M.-N., Doerflinger, E., Collard, P., Masson, F., Meynadier, R., Nahmani, S., Koité, M., Gaptia Lawan Balawan, K., Didé, F., Ouedraogo, D., Pokperlaar, S., Ngamini, J.-B., Lafore, J.-P., Janicot, S., Guichard, F., and Nuret, M.: West African Monsoon observed with ground-based GPS receivers during African Monsoon Multidisciplinary Analysis (AMMA), J. Geophys. Res. 113, number D21105, doi:10.1029/2008JD010327, 2008.

Boehm, J., Werl, B., and Schuh, H.: Troposphere mapping functions for GPS and very long baseline interferometry from European Centre for Medium-Range Weather Forecasts operational analysis data. J. Geophys. Res. 111, B02406, doi:10.1029/2005JB003629, 2006.

Brenot, H., Neméghaire, J., Delobbe, L., Clerbaux, N., Meutter, P., Deckmyn, A., Delcloo, A., Frappez, L., and Van Roozendael, M.: Preliminary signs of the initiation of deep convection by GNSS. Atmos. Chem. Phys. 13, 5425–5449, 2013.

Chen, G. and Herring, T.A.: Effects of Atmospheric Azimuthal Asymetry on the Analysis of Space Geodetic Data. Geophys. Res. Lett. 102, 20489–20502, doi:10.1029/97JB01739, 1997.

Douša, J., Dick, G., Kačmařík, M., Brožková, R., Zus, F., Brenot, H., Stoycheva, A., Möller, G., and Kaplon, J.: Benchmark campaign and case study episode in central Europe for development and assessment of advanced GNSS tropospheric models and products, Atmos. Meas. Tech., 9, 2989-3008, https://doi.org/10.5194/amt-9-2989-2016, 2016.

Douša, J., Václavovic, P., and Eliaš, M.: Tropospheric products of the second European GNSS reprocessing (1996-2014), Atmospheric Measurement Techniques, 10, 3589–3607, doi:10.5194/amt-10-3589-2017, 2017.

Dow, J., Neilan, E., and Rizos, C.: The International GNSS Service in a changing landscape of Global Navigation Satellite Systems. J. Geod. 83(3), 191–198, 2009.

Farr, T. G., Rosen, P. A., Caro, E., Crippen, R., Duren, R., Hensley, S., Kobrick, M., Paller, M., Rodriguez, E., Roth, L., Seal, D., Shaffer, S., Shimada, J., Umland, J., Werner, M., Oskin, M., Burbank, D., and Alsdorf, D.: The Shuttle Radar Topography Mission, Rev. Geophys., 45, RG2004, doi:10.1029/2005RG000183, 2007.

Heki, H., Ryota, S., and Shimada, S.: GNSS climatology : origins of atmospheric delay gradients. EGU General Assembly, 8 April 2019.

IERS Conventions. Petit, G. and Luzum, B. (eds.).: (IERS Technical Note ; 36) Frankfurt am Main: Verlag des Bundesamts für Kartographie und Geodäsie, ISBN 3-89888-989-6, 2010.

Iwabuchi, T., Miyazaki, S., Heki, K., Naito, I., and Hatanaka, Y.: An impact of estimating tropospheric delay gradients on tropospheric delay estimations in the summer using the Japanese nationwide GPS array, Journal of Geophysical Research, 108, D10, 4315, doi:10.1029/2002JD002214, 2003.

Kacmarik, M., Dousa, J., Zus, F., Vaclavovic, P., Balidakis, K., Dick, G., and Wickert, J.: Sensitivity of tropospheric GNSS gradients to processing options. Ann. Geophys. Discuss., https://doi.org/10.5194/angeo-2018-93, 2019.

MacMillan, D.S. and Ma, C.: Using meteorological data assimilation models in computing tropospheric delays at microwave frequencies. Phys. Chem. Earth 23(1), 97-102, 1998.

Meindl, M., Schaer, S., Hugentobler, U., and Beutler, G.: Tropospheric gradient estimation at CODE: Results from global solutions. J. Meteorol. Soc. Jpn. 2004;82:331–338. doi: 10.2151/jmsj.2004.331, 2004.

Morel, L., Pottiaux, E., Durand, F., Fund, F., Boniface, K., Oliveira, P.-S., and Van Baelen, J.: Validity and behaviour of tropospheric gradients estimated by GPS in Corsica. Adv. Space Res., http://dx.doi.org/10.1016/j.asr.2014.10.004, 2014.

Schmid, R., Steigenberger, P., Gendt, G., Ge, M., and Rothacher, M.: Generation of a consistent absolute phase center correction model for GPS receiver and satellite antennas. J. Geophys. Res. 81, 781–798, 2007.

Tregoning, P., Boers, R., O'Brien, D., and Hendy, M.: Accuracy of Absolute Precipitable Water Vapor Estimates from GPS Observations. J. Geophys. Res. 103, 28701–28710, doi:10.1029/98JD02516, 1998.

Willis, P., Bar-Sever, Y. E., and Bock, O.: Estimating horizontal tropospheric gradients in DORIS data processing, preliminary results. IAG Symp 136, 1011–1017, 2012.

Zumberge, J. F., Heflin, M .B., Jefferson, D.C., Watkins, M. M., and Webb, F. H.: Precise Point Positioning for the Efficient and Robust Analysis of GPS Data from Large Networks. J. Geophys. Res. 102, 5005-5017, 1997.

Zhou, F., Li, X., Li, W., Chen, W., Dong, D., Wickert, J., and Schuh, H.: The Impact of Estimating High-Resolution Tropospheric Gradients on Multi-GNSS Precise Positioning, Sensors, 17, 756, doi:10.3390/s17040756, 2017.

Zus, F.; Douša, J.; Kačmařík, M.; Václavovic, P.; Balidakis, K.; Dick, G.; Wickert, J. Improving GNSS Zenith Wet Delay Interpolation by Utilizing Tropospheric Gradients: Experiments with a Dense Station Network in Central Europe in the Warm Season. Remote Sens. 2019a, 11, 674.

Zus, F.; Douša, J.; Kačmařík, M.; Václavovic, P.; Dick, G.; Wickert, J. Estimating the Impact of Global Navigation Satellite System Horizontal Delay Gradients in Variational Data Assimilation. Remote Sens. 2019b, 11, 41

Figure Captions

Fig. 1. Map of the 52 permanent GPS stations considered with a zoom on three particular areas. © Google Maps.

Fig. 2. Spatial distribution of the horizontal gradients along the year 2015 for the station CRAL located in French Pyrenees. The origin corresponds to the location of the GNSS permanent station.

Fig. 3. Spatial distribution of the horizontal gradients along the year 2015 for the station CRAL located in French Pyrenees. The cloud points are counted in each 30° azimutal sector and represented by their sum. All the points are connected by a red curve to represent the spatial distribution.

Fig. 4. Example of relief around the UNSA station located in Argentina near the Andes (class 1). The spatial distribution of the relief is represented by three curves corresponding to three distances from the station (20, 40 and 60 km) to identify the highest elevation point in all the directions. Distance from the centre is proportional to the height difference between the

station elevation and the highest elevation point. The four circles drawn represent height differences of 1000 m, 2000 m, 3000 m and 4000 m respectively.

Fig. 5. Gradient orientation curve (blue) and relief curves (red, green and purple) around the station ARAN located in France near the Alps considering three distances from the station (20, 40 and 60 km) for the relief representation.

Fig. 6. Relative location of mountains from the station (top charts). Gradients and relief curves (bottom radar charts centred on station location) for class 1 stations: GHER (Himalaya), POL2 (Nepal), P572 and P467 (California near Sierra Nevada). Red curve (filled with pink) represents the gradient and the other curves represent the relief at different distances from the station: blue for 20 km, orange for 40 km and green for 60 km. Y axis legend corresponds to the elevation in m. (scale is different for GHER as it is situated in Himalaya, with height difference up to 6 km). Other axis legend (at 135° azimuth) corresponds to the sum of gradient.

Fig. 7. Location of mountains relative to the 'class 3' GNSS station MICH located in California near the Sierra Nevada (left). Horizontal gradient and relief curves (right). Red curve (filled with pink) represents the gradient and the other curves represent the relief at different distances from the station: blue for 20 km, orange for 40 km and green for 60 km. Y axis legend corresponds to the elevation in m. Other axis legend (at 135° azimuth) corresponds to the sum of gradient.

Fig. 8. Location of mountains relative to the 'class 4' GNSS station BZRG located in Italia near the Dolomites (left). Horizontal gradient and relief curves (right). Red curve (filled with pink) represents the gradient and the other curves represent the relief at different distances from the station: blue for 20 km, orange for 40 km and green for 60 km. Y axis legend corresponds to the elevation in m. Other axis legend (at 135° azimuth) corresponds to the sum of gradient.

Fig. 9. Correlation coefficient for stations of class 1 and 2 between the gradient direction and the relief curves at 60 km from the station.

Fig. 10. Schematic path delay across troposphere of a GPS signal in the presence or not of mountains.

Fig. 11. Bimonthly variations of the mean tropospheric gradients sum all along the year 2016 for 5 stations. The dashed line represents the relief around the station estimated at 60 km from the station.

Fig. 12. Average of diurnal variations of gradients for 2016 for 5 stations. The dashed line represents the topography around the station at a distance of 60 km from the considered station.

Fig. 13. Radar charts of gradient curve (red curve filled with pink) and relief curves (dark blue, orange and green curves) for 3 couple of neighbouring stations (GHER and BESI (class 1) located in Nepal near Himalaya; POL2 (class 1) and CHUM (class 2) located in Kazakhistan near Alaa-Too mountains; KOSM and APNT (class 2) located in Hawai).